Applied Geography 53 (2014) 341–353

Contents lists available at ScienceDirect

Applied Geography

journal homepage: www.elsevier.com/locate/apgeog

Geographically weighted regression of the urban heat island of a small city

Danijel Ivajnšič [a, *], Mitja Kaligarič [a], Igor Žiberna [b]

[a] Department of Biology, Faculty of Natural Sciences and Mathematics, University of Maribor, Koroška 160, SI-2000 Maribor, Slovenia
[b] Department of Geography, Faculty of Arts, University of Maribor, Koroška 160, SI-2000 Maribor, Slovenia

Keywords:
Geographically weighted regression
Ljutomer
Ordinary least squares
Temperature differences
Urban heat island

A B S T R A C T

Despite differences in regional climates, cities world-wide have developed one common characteristic - the urban heat island (UHI). Its magnitude is related to city size, especially under cloudless sky conditions on a regional basis, although individual cities may be impacted by such local factors as proximity to large water bodies or prevailing winds. The UHI pattern in the small city of Ljutomer was examined in order to assess its intensity and morphology and to test the utility of the geographically weighted regression (GWR) method in modeling the regression relationships between mean air temperature and related influence factors in this small-scale urban example. Significant differences in mean air temperature between urban and rural areas were measured. It turned out that built-up areas in Ljutomer are on average 1 °C warmer than the rural surroundings in winter time. The regression analyses confirmed the important role of local non-stationary explanatory variables - distance to urban area, topographic position index and land-cover diversity - and global stationary variables - building volume per area and northness - in explaining spatial variation in mean air temperature. The relationships between mean air temperature and these five explanatory variables produced an overall model fit of 91%, utilizing the semiparametric GWR method, which was tested on the smallest scale so far published.

Introduction

The urban heat island (UHI) effect is among the best expressions of the impact of human activity on local Climate (Hinkel, Nelson, Klene, & Bell, 2003). More than 150 years of urban climate studies (Howard, 1820) have shown that thermal, optical and geometric properties of urban surfaces affect heat absorptive and radiative properties and lead to the UHI effect (Feyisa, Dons, & Meilby, 2014; Gartland, 2008; Voogt & Oke, 2003). Urban warming is a manifestation of the direct and indirect alteration of the energy budget in the urban boundary layer. The direct impact is easily visualized as the transformation of stored chemical energy, typically in the form of high-quality fossil fuel. Known as anthropogenic heat, energy is converted to alternate forms to generate heat for buildings and steam for electrical power generation, to power motorized vehicles and drive industrial processes. Although several energy transformations may be involved, the stored chemical energy is eventually dissipated into the atmosphere as sensible heat. Because human activities are concentrated in urban areas, a net flux of heat into the atmosphere is often detectable (Hinkel et al., 2003). The indirect impact is more complex (Arnfield, 2003). This includes land-cover transformation, mainly the replacement of natural vegetation and agricultural land by an impervious surface associated with urban land use (Buyantuyev & Wu, 2010). In response to removal of the natural land cover and the introduction of artificial materials (e.g., concrete, asphalt, tiles, metals, etc.), the radiative, thermal and moisture conditions as well as roughness and emissivity of the surface (and consequently the atmosphere above) change dramatically (Li, Wang, Wang, Ma, & Zhang, 2009; Roth, 2002). As a result, alternation of surface energy fluxes occurs, with a consequent increase in the Bowen ratio (the ratio of sensible to latent heat fluxes), which, in turn, causes an increase in temperatures on and above every urban surface (Oke, 1982; Stull, 1988). The concentration of aerosol and gaseous pollutants in the urban canopy can affect radiation exchange between the surface and the atmosphere. Stewart, Stenz, and Gottinger (2011) pointed out that elevated air temperatures are also known to help induce the chemical reactions that produce tropospheric ozone, whereas Johnson and Wilson (2013) reported that heat-

* Corresponding author. Tel.: +386 2 2293 730.
E-mail addresses: dani.ivajnsic@uni-mb.si (D. Ivajnšič), mitja.kaligaric@uni-mb.si (M. Kaligarič), igor.ziberna@um.si (I. Žiberna).

http://dx.doi.org/10.1016/j.apgeog.2014.07.001
0143-6228/

related morbidity is congruent with higher UHI intensity levels, particularly in poor urban areas within large agglomerations in the USA. All these changes (direct and indirect) modify the energy balance, water balance and air circulation patterns of the city, although the impact of these factors varies between cities because the geographic setting, urban morphology, patterns of urban land use, and available construction materials are city specific (Landsberg, 1981). However, the main characteristics of the specific city climate in general are as follows: higher air temperatures, mainly at night and in the mornings before sunrise (mid latitudes); lower relative air humidity; lower mean wind velocity and higher levels of air pollution (Žiberna, 2006). Research on the UHI has typically focused on tropical and mid-latitude cities for the dual purposes of understanding the dynamics of the energy balance in the urban boundary layer (Oke, 1987), and application to issues related to urban pollution, energy conservation, and prevention of heat-related health problems or deaths (Buechley, Truppi, & Van Brugg, 1972; Hinkel et al., 2003; Oke, Spronken-Smith, Jauregiu, Grimmond, 1999; Rosenfeld, Akbari, Romm, & Pomerantz, 1998).

UHI develops primarily at night throughout the year and depends heavily on weather conditions (Arnfield, 2003; Buyantuyev & Wu, 2010; Souch & Grimmond, 2006). The intensity of UHI changes seasonally (Fezer, 1994). UHI is, in northern and mid geographical regions (Northern Hemisphere), more pronounced during winter (Hinkel et al., 2003; Žiberna, 2006). In contrast to this, in arid and semi-arid environments, where UHI intensity is dependent on high variability in vegetation (Jonsson, 2004), the UHI maximum usually appears in summer or in the dry season. However, it is known that urban vegetation eases surrounding microclimates through increased latent heat exchange, shade and lack of heat from combustion sources (Buyantuyev & Wu, 2010; Jonsson, 2004; Spronken-Smith & Oke, 1998). Urban greenspaces, parks and water bodies therefore have a cooling influence on the elevated air temperature, and these effects can extend hundreds of meters beyond their boundaries (Choi, Lee, & Byun, 2012; Spronken-Smith & Oke, 1998; Upmanis, Eliasson, & Lindqvist, 1998). Contrary to this, Feyisa et al. (2014) reported a maximum park cooling distance of only 240 m and a maximum park cooling intensity of 6.72 °C in Addis Ababa (Ethiopia) and concluded that the cooling effect of urban green space is mainly determined by species group, canopy cover, size and the spatial design of parks.

According to Oke (1982), two layers can be distinguished in the urban atmosphere: the urban canopy layer (UCL), containing air between the urban roughness elements (mainly buildings), and the urban boundary layer (UBL), which is situated directly above the UCL. The latter is a local or mesoscale concept whose characteristics are governed by the nature of the whole urban area. This study, following the research of Balazs et al. (2009), focuses on the heat island in the UCL, where most human activities usually take place. The first attempts to analyze UHI structure were based on manually interpolated isotherm maps (Duckworth & Sandberg, 1954). More sophisticated interpolation algorithms became popular with increasing access to effective computers and the development of accessible geographic information systems (GIS) software (Alcoforado & Andrade, 2006; Bottyán and Unger 2003; Svensson, Eliasson, & Holmer, 2002; Szymanowski & Kryza, 2012; Vicente-Serrano, Cuadrat-Prats, & Saz-Sánchez, 2005). Unger, Savić, and Gal (2011) reports that most recent studies on the spatial characteristics of UHI are based on multidimensional interpolation algorithms, with multiple linear regression (MLR) being the most often applied. Although global multivariate regression relationships are relatively well-established, the statistical analyses of previous studies have commonly been aspatial, neglecting the locational information associated with each sample site (Foody, 2003). Dutilleul and Legendre (1993) pointed out that observed geographical and ecological patterns and processes in nature, unlike universal physical laws, tend to be spatially variable. This phenomenon is often referred to as spatial non-stationarity (Li, Zhao, Miaomaio, & Wang, 2010). Multiple regression analysis such as the Ordinary Least Squares (OLS) model is based on the assumption of independence of observations, resulting in a failure to capture the spatial dependence of the data when it is applied to geo-referenced data analyses (Li et al., 2010). Brunsdon and Fotheringham developed a local regression technique, Geographically weighted regression (GWR), to overcome this limitation of the OLS method (Brunsdon, Fotheringham, & Charlton, 1996; Fotheringham, Brunsdon, & Charlton, 2002). There have been several recent works where non-stationary statistical methods (such as GWR) are applied to model or analyze UHI (Farber & Paez, 2007; Su, Foody, & Cheng, 2012; Zhou and Wang 2001). Spatial variation in the relationship between variables both at and between spatial scales is reported in the recent literature for studies with spatially distributed environmental data. The studies by Foody (2003, 2004); Propastin, Kappas, and Erasmi (2008) showed that the predictive power as well as the rank order of explanatory variables in spatial models between remotely sensed data and climatic parameters is a function of scale. Therefore, GWR is not a problem-free statistical method, major concerns are focused on issues such as kernel and bandwidth selection. However, its potential for dealing with spatial non-stationary issues has been validated (Foody, 2003; Li et al., 2010).

Understanding and quantifying UHI and its factors are important steps toward improving the quality of life of urbanites and achieving urban sustainability in all types of cities across the globe (Grimm et al., 2008; Wu, 2008). While most studies about UHI focus on medium or large urban areas, our main objective in this study is oriented towards assessment of the intensity and morphology of an UHI event during winter time, in a small city named Ljutomer (a) and to test the utility of GWR in modeling the regression relationships between mean air temperature and related influence factors in this small-scale urban example (b).

Study site

Ljutomer is located in the NE part of Slovenia (46°31′N, 16°11′E), on the western outskirts of the Great Pannonian Basin (Fig. 1 A, B).The city has developed in the transition zone from the surrounding Tertiary hills to the Quaternary plain of the Ščavnica river. Most of the city area lies on the river plain of the Ščavnica, (from 172 to 180 m a.s.l.), except the new suburban part in the SW, which stretches to the warm southern slopes of Kamenščak hill (64 m relative elevation difference) (Fig. 1 C). The Ščavnica river (2–5 m wide) and its narrow regulation canal cross the city area. The climatic influence of these narrow water streams is probably negligible. The east side of the city is bounded by the railway, which represents a sharp line between urban and rural areas (Fig. 1 C).

The climate in the region around Ljutomer is under a strong continental influence, due to its geographical position next to the Great Pannonian Basin. Yearly and daily air temperature amplitudes therefore reach the maximum value in the country (10.4 °C; 30-year average from 1971 to 2000; ARSO, 2006). The mean air temperature is the second highest (9.6 °C from 1971 to 2000) after the Sub-Mediterranean region in the SW part of Slovenia (12.8 °C from 1971 to 2000) (ARSO, 2006; Ogrin, 2009). The surrounding hills exhibit slightly milder continental traits, particularly in the thermal zone, where the minimum temperatures are significantly higher (Ogrin, 2009). The NE parts of Slovenia receive annually a mean precipitation amount of 800–1000 mm (based on data from 1971 to 2000) (ARSO, 2006; Ogrin, 2009). Most of this precipitation falls in summer (more that 1/3 of the annual rate) and just 15% in winter.

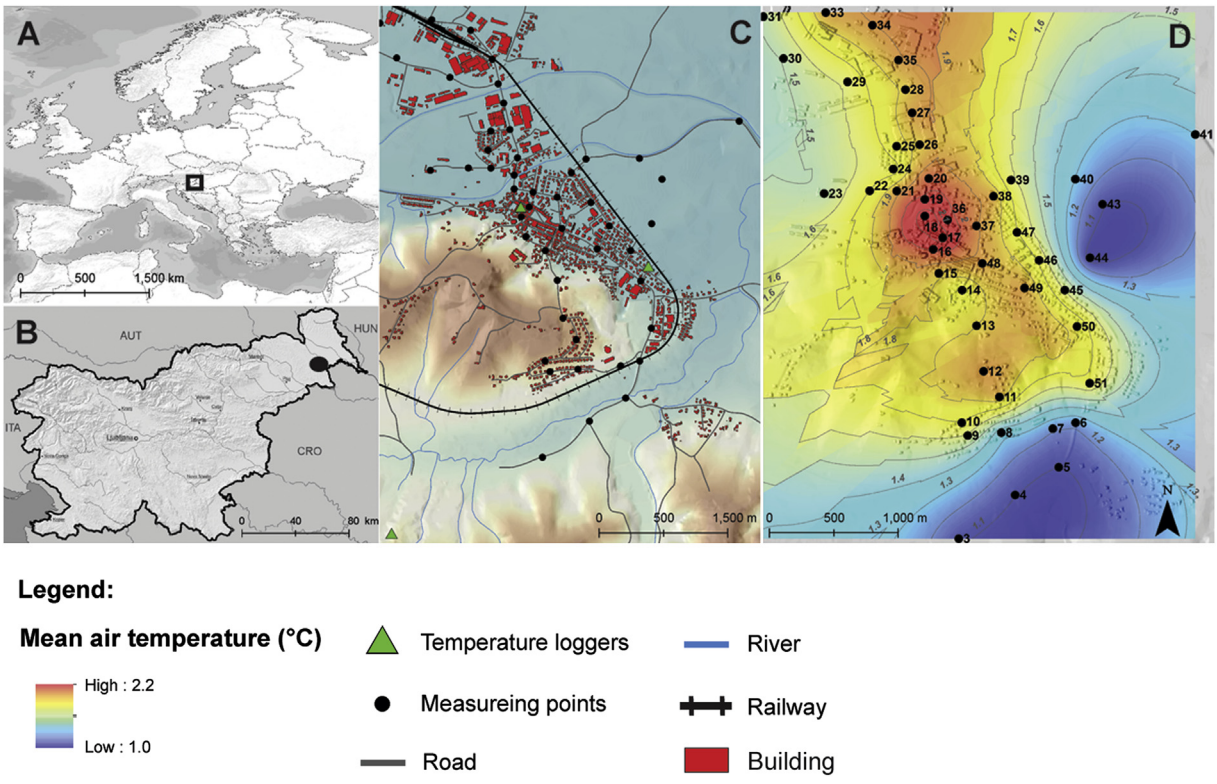

Fig. 1. Location of the city of Ljutomer in Europe (A) and Slovenia (B). City structure and the surrounding topography together with the distribution of measuring points and temperature loggers (C) and the mean air temperature raster surface with ordinary kriging interpolation overlayed on the digital surface model (D).

Slovenian geographers consider this climate as the Sub-Pannonian climate. According to the Köppen-Geiger climate classification, the region around Ljutomer is categorized as the Cfb climate (a temperate warm climate with warm summers and adequate rainfall throughout the year, always with a surplus water budget) (Kottek, Grieser, Beck, Rudolf, & Rubel, 2006).

The origin and development of Ljutomer are similar to that of other Slovenian medieval market towns and cities. In 1927 Ljutomer officially became a city, with a typical medieval structure (Belec, 1995). After the Second World War ended the regulation of the Ščavnica river, the city **sprawled** around the quadrilateral market in a N and SE direction along the major road, with the urban policy and architecture typical of all countries with socialist regimes. Today, the northern section is mainly industrial (flat, horizontal buildings not higher than 10 m); the eastern section, between the old medieval center and the railway, is occupied by detached houses and some tall apartment buildings (mostly below 6 stories). The new section of the small city, occupied by family houses, is developing on the southern slope of nearby Kamenščak hill in the SW outskirts (Fig. 1 C).

Methodology

Temperature measurements

Because the micro location of the measuring stations, in the case of UHI research, is a very important factor, and the nearest meteorological station is located 8 km from Ljutomer city (in the hills of Jeruzalem 345 m a.s.l. in a thermal belt), we were forced to use our own measuring equipment. We installed three temperature loggers (Plug&Track Thermo Button 22 L; 30 min measuring interval; temperature accuracy = ±0.5 °C; resolution = 0.1 °C) in a Davis Radiation Shield, according to the built-up ratio gradient criteria (one in the city center (3; 172 m a.s.l.), one in the SE part of the city which is occupied by detached houses (2; 175 m a.s.l.) and one in the settlement 3 km away), which represents a more or less rural area (1; 214 m a.s.l.), in order to track temperature differences between urban and non-urban areas (Fig. 1 C). All temperature loggers were installed 2 m above similar ground (grass) in a northern direction. Altogether, 17,208 measurements (5736 in each) were taken between 1.12.2008 and 31.3.2009. These data were then compared in an ANOVA statistical analysis together with Tukey's Pairwise Test and Duncan's New Multiply Range Test, using *R* statistical software (R Development Core). A meteorological station (Technoline WS-3600) was installed in the settlement for determination of weather types according to Čadež (1949). For measurements of UHI intensity and morphology, temperature data were collected by mobile measurements in the urban area of Ljutomer and in the surroundings, at 47 randomly dispersed points (Mean Nearest Neighbor = 172 m), between 1.12.2008 and 31.3.2009 (Fig. 1 C) with a TFD digital control thermometer (Temperature accuracy = 0.5 °C; resolution = 0.1 °C). According to Oke (2004), the circle of influence on a screen level (~1.5 m) temperature is believed to have a typical radius of about 0.5 km. The required data were collected by car on the assigned route. This type of mobile measurement is widespread in observing urban climate parameters (e.g., Balazs et al., 2009; Moreno-Garcia, 1994; Oke & Fuggle, 1972), although the ventilation effect caused by the speed of the car must be considered as an error. All 47 points were measured 30 times, and each of these measurement runs took 45 min to complete at around 7:00 am. Based on experience from previous studies, we measured the temperature differences in Ljutomer at around the expected time of the daily maximum development of the UHI (Balazs et al., 2009; Bottyan, Kircsi, Szegedi, & Unger, 2005; Oke, 1981, 1987; Unger, 2004). Owing to logistical limitations, mobile measurements were carried out constantly at around 7:00

am, which means that solar radiation did influence some results (sunrise before 7:00 am), in particular those on the exposed slopes of Kamenščak hill in mid-February and in March 2009. Altogether 6 different weather types (12× in A1 – anticyclonic type; 4× in A2 – anticyclonic type with fog during the day; 5× in AD – anticyclonic-advective type; 3× in C – cyclonic type; 1× in CD – cyclonic-advective type and 5× in D – advective tape), according to the classification by Čadež, were considered in this study.

Selection of regression variables

Dependent variable

The mean air temperature at each of the 47 measuring points, in 30 measurement days, was calculated and used as the dependent variable. 10 points were located outside of the city and can be characterized as agricultural, consisting mainly of fields and grasslands (3, 4, 5, 6, 7, 39, 40, 41, 43 and 44) (Fig. 1 C and D). For visual interpretation, an ordinary kriging interpolation method was used (in the 250 m radius zone around the points), within the ArcGIS 9.3 Spatial Analyst Tool (ESRI, 2010) (Fig. 1 D). All further analyses were performed only with actual measurements (point data).

Explanatory variables

Distance to urban area (DIS2UA)

Primarily, the built-up ratio or artificially covered surface ratio, which horizontally characterizes the surface of a settlement (streets, pavements, parking lots and roofs) (Balazs et al., 2009; Li et al., 2010; Unger et al., 2011) was determined on a 40 × 40 m grid, using a vectorized city land register for 2007 (GURS, 2007), validated with the Normalized Difference Vegetation Index (NDVI) extracted from 2006 near-IR orthophoto imagery (DOF100IR; horizontal resolution of 1 m) (GURS, 2007). The land register polygons, which represented the artificially covered surface, were converted to 1 × 1 m raster with ArcGIS 9.3 Conversion Tools (ESRI, 2010). Then each pixel was transformed into a point representing the pixel centroid. Finally, a 40 × 40 m point density surface was calculated with the Spatial Analyst Tool in ArcGIS. Additionally, NDVI was calculated using the equation (Gallo, Owen, Easterling, & Jamason, 1999; Tucker, 1979): NDVI = (IR − R)/(IR + R). According to the research of Grigillo, Kosmatin Fras, and Petrovič (2011), we actually calculated a modified NDVI because the red and near-infrared bands in DOF100IR are decoded as green and red bands. However, the meaning of these modified NDVI is the same as the real NDVI, where the value varies between −1 and +1 depending on the surface cover (vegetation, water) (Lillesand & Kiefer, 1987, p. 705). In the case of bare rock, asphalt and concrete, the value is around zero, since the reflectance of red and near-infrared are nearly equal (Balazs et al., 2009). A built-up area, on the 40 × 40 m grid, could be expressed from the modified NDVI map and then compared (Image Similarity Statistics) to the built-up point density surface calculated from the city land register.

Secondly, the final built-up area raster represented the base for calculating the *DIS2UA* variable, considering a built-up threshold value of 0.7 as the boundary between urban and non-urban areas. In this regard, a boolean raster was calculated showing the urban area. The Euclidean distance tool in ArcGIS 9.3 was applied in the next step to determine the *DIS2UA* variable. Finally, the values of the 40 × 40 m distance to the urban area raster were attributed to all 47 measuring points as the first explanatory variable.

Building volume per area (BVOL)

The national Register of buildings for 2014 (a digital vector database), owned by the Ministry of Infrastructure and Spatial Planning (GURS, 2014), was used in order to determine the ground plan of each building in Ljutomer. Building height, measured by photogrammetric methods with an average vertical accuracy of ±30 cm is one of the attributes of this vector database and represents the difference between surface elevation and the highest point of the building. Accordingly, the *BVOL* (without roofs) in the 40 × 40 m grid could be calculated and attributed to all 47 measuring points as the second explanatory variable.

Land-cover diversity (LCD)

In order to consider the various land-cover types which are present in and around the city, we used the free national vector database of land-use for 2009 (GERK 2012), available at http://rkg.gov.si/GERK/(17.04.2012). To satisfy the requirements of GWR, Shannon's Diversity Index based on land-cover types was calculated with the use of Land Facet Tools for ArcGIS, designed by Jenness Enterprises. Shannon's Index (*H*) is a measure of diversity and evenness that reflects both the number and the balance of unique values within an area (in this case, the area is a moving window) (Jenness, Brost, & Beier, 2013). *H* values increase both with the number of classes observed and with how evenly distributed they are. The following equation according to Shannon and Weaver (1963) was used:

$$H = -\sum_{n=1}^{S} p_i \ln p_i$$

where p_i is equal to the proportion of land-cover categories in the area of interest and then multiplied by the natural logarithm of this proportion ($\ln p_i$). The vector data of land-use were transformed into raster format in order to run the analyses, and a 40 m radius size (circular neighborhood) was chosen for the moving window approach. A new raster map with Shannon's index values emerged. The pixel values were than extracted for all 47 measuring points as the next explanatory variable called *LCD*.

Northness (NORTHNESS)

The slope aspect of the land surface strongly affects the amount of solar radiation intercepted, and its spatial variation is therefore an important natural determinant of land surface temperature and consequently also of air temperature during the day (Li et al., 2010). In general, south-facing slopes have the highest land surface temperature values, and the value decreases consistently as the aspect changes from south to north in the Northern Hemisphere (Sheng, Wilson, & Lee, 2009). In all GIS software, the digital elevation model (DEM) based aspect is mainly expressed in circular data; large values may be very close to small values. To get a linear relationship between mean air temperature and aspect and to satisfy the requirements of GWR, aspect (originally represented by the compass direction of a slope) was transformed using the trigonometric function (*NORTHNESS* = cos (aspect)) (Roberts, 1986). *NORTHNESS* will be close to −1 when the aspect is southward, close to 1 when the aspect is generally northward, and close to 0 when the aspect is eastward or westward. We calculated aspect, based on a 5 m resolution digital surface model (DSM), developed on the basis of the previously mentioned register of buildings (GURS, 2014) and a 5 m resolution DEM (GURS, 2010). The building height raster was combined with the DEM using the Raster

calculator tool in ArcGIS 9.3. Finally the DSM based *NORTHNESS* was calculated on a 40 × 40 m grid and applied to all 47 measuring points in order to include the shading effect of the built-up area.

Topographic position index (TPI)

Relative elevation is, of course, an important determinant of air temperature in the city if it is surrounded whether by convex or concave topography. Ljutomer stretches partway to nearby Kamenščak hill; this is why we chose to include *TPI* as an explanatory variable in order to consider possible cold air drainage flows that might disturb the overall pattern of the UHI. The *TPI* is simply the difference between a cell elevation value and the average elevation of the neighborhood around that cell. Positive values mean the cell is higher than its surroundings, while negative values mean it is lower (Jenness et al., 2013). *TPI* units are in elevation units, such that a *TPI* value of 10 would mean that this particular cell is 10 units (generally meters) higher than the average elevation of the neighborhood. It should be emphasized that *TPI* values are strongly scale-dependent. *TPI* was calculated with the use of Land Facet Tools for ArcGIS, designed by Jenness Enterprises, based on the DEM (GURS, 2010), with a 300-m circular type neighborhood on a 40 × 40 m grid and extracted to all 47 measuring points as the last explanatory variable.

Hot Spot Analysis, OLS and GWR

In order to statistically test the morphology and intensity of the urban heat island in Ljutomer, a Hot Spot Analysis (Getis-Ord Gi* statistic) with the 47 measuring points using ArcGIS 9.3 Spatial Analyst Tools (ESRI, 2010) was performed (Fig. 3). The distance threshold value (430 m) for this test was statistically determined using the Incremental Spatial Autocorrelation tool in ArcGIS (ESRI, 2010). The resultant z-scores and *p*-values of the Getis-Ord Gi* statistic indicate where features with either high or low values cluster spatially. The Gi* statistic returned for each feature in the dataset is a z-score. For statistically significant positive z-scores, the larger the z-score, the more intense the clustering of high values (a hot spot). For statistically significant negative z-scores, the smaller the z-score, the more intense the clustering of low values (a cold spot) (ESRI, 2010; ArcGIS Help). Secondly, to highlight the good performance of the GWR model, the OLS model, one of the classic global regression analysis techniques, was performed in advance using ArcGIS (Li et al., 2010). *DIS2UA*, *BVOL*, *NORTHNESS*, *LCD* and *TPI* were chosen as explanatory variables for prediction of the dependent variable mean air temperature. In order to get a properly specified OLS model, the following tests were performed: Adjusted R-Squared (R^2), corrected Akaike Information Criteria (AICc), Jarque-Bera *p*-value (JB), Koenker's studentized Breusch-Pagan *p*-value (BP), Variance Inflation Factor (VIF), and Global Moran's I *p*-value (MI) using ArcGIS (ESRI, 2010). The OLS method can be applied to spatial data under the assumption of spatial non-stationarity and location-independency. These conditions are usually hard to meet, especially in the field of meteorology and climatology, where many processes can be considered as spatially unstable (Szymanowski & Kryza, 2012). Therefore, a local statistical technique may be more appropriate for non-stationary cases (Foody, 2003, 2004, 2005; Fotheringham et al., 2002; Maselli, 2002; Su et al., 2012). In 2002 Fotheringham et al. gave a detailed description of the GWR algorithm and the principle. It is a non-parametric model of spatial drift that relies on a sequence of locally linear regressions to produce estimates for every point in space by using a subset of information from nearby observations (Szymanowski & Kryza, 2012). This geographical weighting is implemented through a spatial kernel function (Gaussian, Poison or Logistic) depending on the data type. Before applying the GWR method, all explanatory variable were tested for geographical variability with the GWR calibrated F-test and the AICc in GWR4 software (Nakaya, Charlton, Fotheringham, & Brundson, 2014), where positive AICc (DIF criterion) values suggest no spatial variability in terms of model selection criteria. Three out of five explanatory variables (*DIS2UA*, *LCD* and *TPI*) exhibited significant spatial non-stationarity (DIFF Criterion > +2) at a 95% confidential level. In this regard a semiparametric GWR method was calibrated with an adaptive Gaussian kernel type, applying the Golden section search function for the best bandwidth size selection based on the AICc criterion value in the GWR4 software (Nakaya et al., 2014). A semiparametric Gaussian GWR model is described as:

$$y_i = \sum_k \beta_k(u_i, v_i)x_{k,i} + \sum_l \gamma_l z_{l,i} + \varepsilon_i$$

where y_i, $x_{k,i}$ and ε_i are, respectively, dependent variable, *k*th independent variable, and the Gaussian error at location *i*; (u_i, v_i) is the *x*/*y* coordinate of the *i*th location; and coefficients $\beta_k(u_i, v_i)$ are varying conditionals on the location. Usually, the first variable is constant by setting $x_{0,i} = 1$, after which $\beta_0(u_i, v_i)$ becomes a geographically varying 'intercept' term. Additionally, $z_{l,i}$ is the *l*th independent variable with a globally fixed coefficient γ_l. Thus, the model mixes geographically local (left part of the equation) and global fixed terms (right part of the equation) and may reduce the model's complexities and enhance its predictable performance (Nakaya et al., 2014). *DIS2UA*, *LCD* and *TPI* were selected as local whereas *BVOL* and *NORTHNESS* as global independent variables. Both models (OLS and semiparametric GWR) were finally tested for overall fit performance and possible GWR over OLS improvement with an ANOVA test (Brundson, Fotheringham, & Charlto, 1999; Fotheringham et al., 2002) in GWR4 software (Nakaya et al., 2014). Finally, the results of both models were also tested for residual spatial autocorrelation in ArcGIS 9.3 with the Moran index (MI).

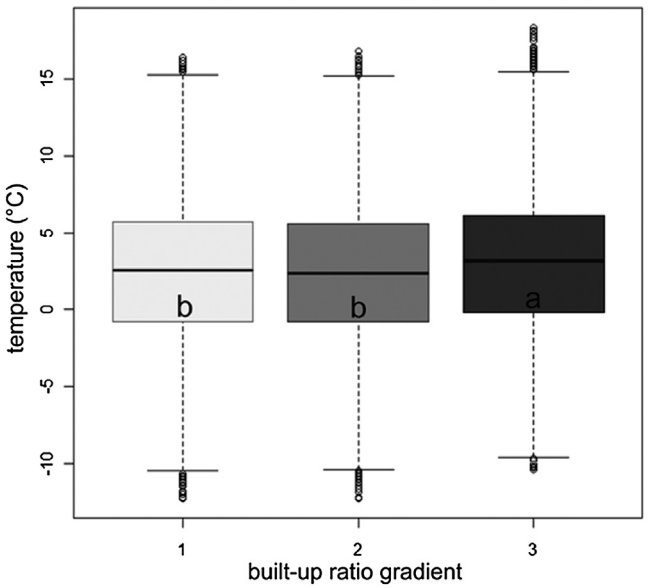

Fig. 2. Differences in air temperature between certain parts of the city according to the built-up ratio gradient. 1 = rural surroundings (low built-up ratio), 2 = "suburban" part in the SE (medium built-up ratio), 3 = city center (high built-up ratio).

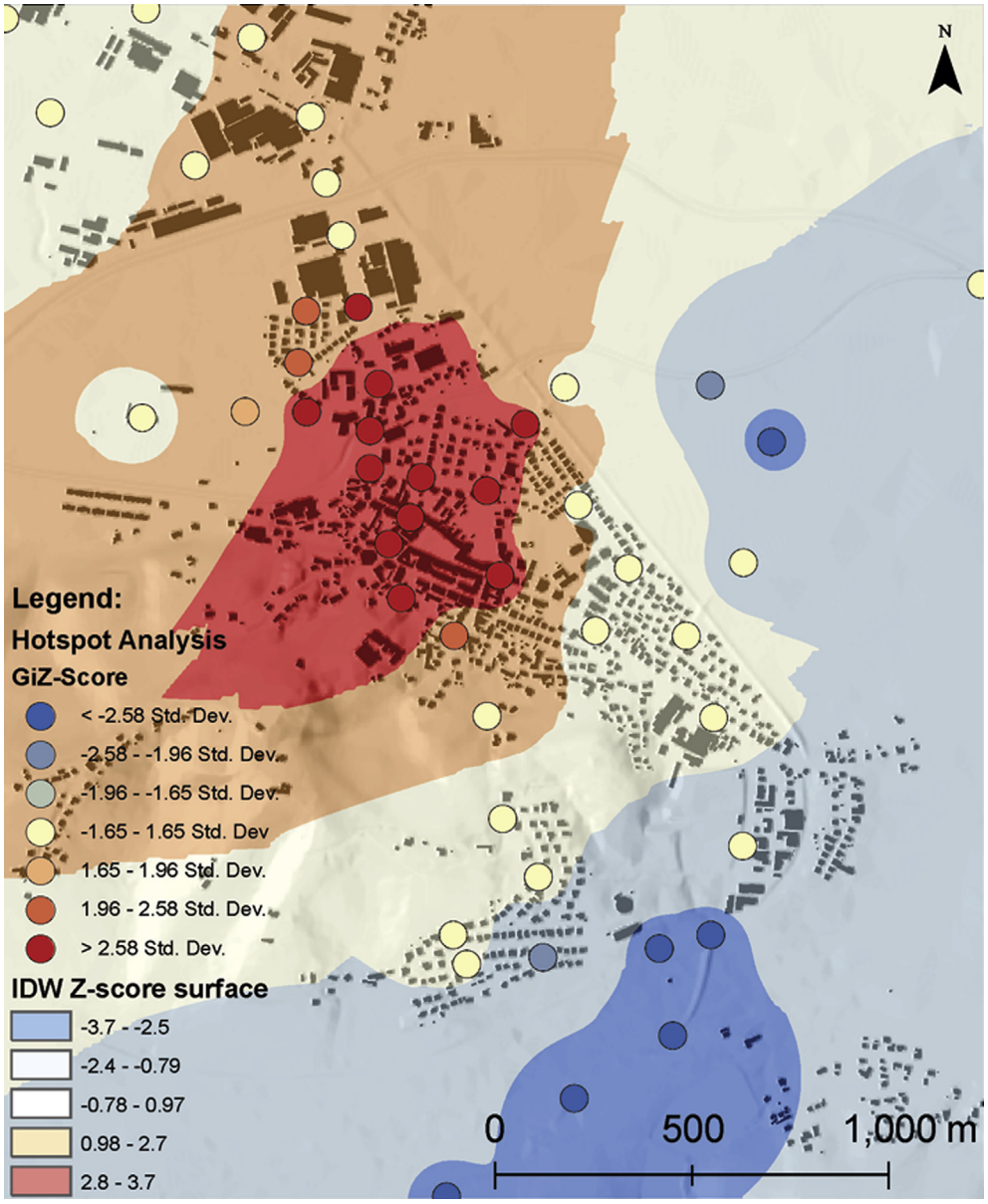

Fig. 3. Hot Spot Analysis with corresponding Z-scores and an interpolated surface of Z-scores using the IDW method.

Results

Differences in air temperature across the built-up ratio gradient

The Levine's Test for Homogeneity of Variance showed that there was no difference in variability of air temperature among these three measuring stations (F value = 0.0995; Pr > F = 0.9053). Additionally, the one way ANOVA analysis, together with Tukey's Pairwise Test and Duncan's New Multiply Range Test, proved that there were differences in the mean air temperature between these three locations (p = 1.009e-15***) (Fig. 2). Both Pairwise tests indicate that there are statistically significant differences in mean air temperature between the measuring station in the area of high built-up ratio (3) and the other two stations (1 and 2). The station located in the city center also had the highest mean air temperature (3.1 °C). Surprisingly, there were no statistically significant differences in mean air temperature between the suburban SE part of the city, which is occupied by detached houses (2), and the rural surroundings (1) of the city (p = 0.797) (Fig. 2). However, the mean air temperature measured in the suburban part of the city was a bit higher (2.4 °C) compared to the settlement representing the rural area (2.3 °C).

Hot and cold spots in the city and its surroundings

The data from the permanent measuring stations (air temperature loggers) proved that there are differences in air temperature across the built-up ratio gradient. Based on that, we tested, in regard to mobile measurements in Ljutomer and its surroundings, whether there exist statistically significant hot and cold spots (if Ljutomer has developed a statistically significant UHI). The Hot Spot Analysis (Getis-Ord Gi* statistic), based on mean air temperature at each measuring point (30 measurements in six different weather types according to Čadež) shows a statistically significant hot spot in the center of Ljutomer, which stretches partway into the northern industrial area (Fig. 3). The measuring points in the rural

vicinity (in the S and E directions) are defined as statistically significant cold spots. The industrial area in the northern part of the city and the new section in the southwest, located on the warm southern slope of Kamenščak hill, do not show a tendency towards clustering according to mean air temperature. As expected, the measuring point located by the confluence of the Ščavnica river and its regulation canal (on the E side of the city) does not show up as a cold spot, regardless of its geographical position in a completely rural area. The effect of water as an air temperature determinant could be considered here (Fig. 3).

Relationships between the dependent and explanatory variables

Bivariate relationships between mean air temperature as the dependent variable and the explanatory variables *DIS2UA*, *BVOL*, *LCD*, *NORTHNESS* and *TPI* are presented in Fig. 4. *DIS2UA* has a negative relation with mean air temperature, as expected. The mean air temperature drops by 0.13 °C with a 100 m distance increment from the built-up area of Ljutomer. 58% of mean air temperature variability is explained by the linear trend. *BVOL* has a positive influence on the mean air temperature. If *BVOL* rises for 1000 m^3, mean air temperature increases by 0.06 °C. 23% of mean air temperature in Ljutomer is explained by this explanatory variable. *LCD* has a much higher linear relation, with 37% of explained variability. With a change of 0.35, the mean air temperature drops by 1 °C. The southern exposed areas in Ljutomer have a slightly higher mean air temperature than those with a northern exposure. The relationship is therefore negative. Although only 9% of the dependent variable is explained by *NORTHNESS*, it is an important variable, mainly explaining higher temperatures in the part of the city that stretches to the slopes of Kamenščak hill. Topographic variability can play a key factor in the spatial pattern of an UHI. The relation between mean air temperature and *TPI* in Ljutomer is slightly positive, which means that convex areas are a bit warmer than concave areas in the city. All explanatory variables exhibited a statistically significant contribution by modeling UHI in Ljutomer (Fig. 4). The multicollinearity test of explanatory variables (the Variance Inflation Factor Test (VIF)) proved that the predictors were not redundant. All VIF values were clearly under the critical value of 7.5, indicating that each of the predictors has a different influence on the dependent variable (Fig. 4).

OLS model vs. semiparametric GWR model

The diagnostics of the OLS model (Table 1) show that overall the OLS model is statistically significant (Joint F-statistic $p = 0.0000$*;

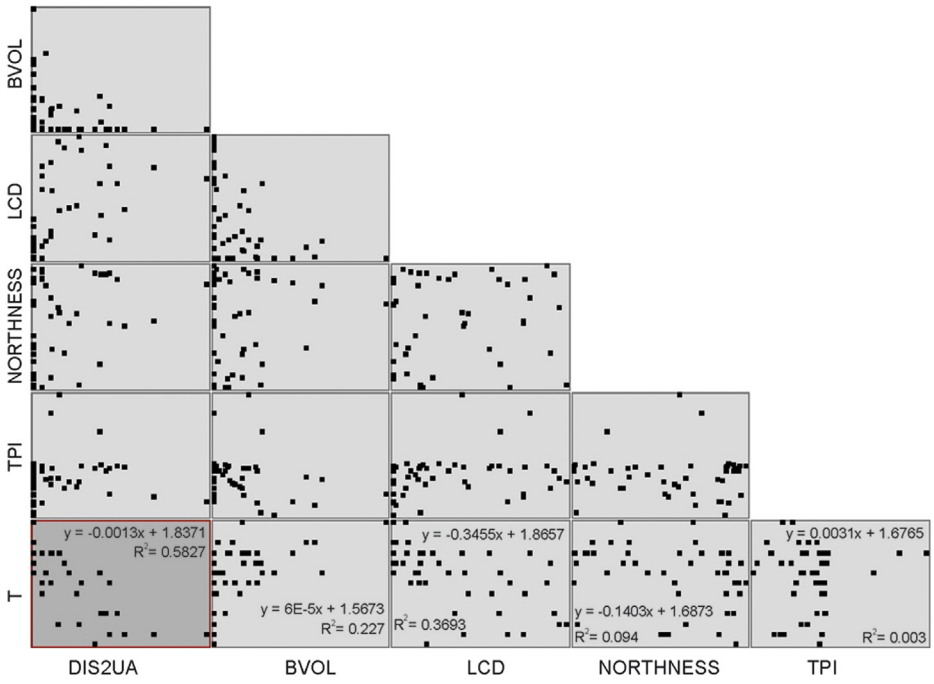

Variable	Variance Inflation Factor (VIF)	Variable significance (p-value)
DIS2UA	1.568	0.0000
BVOL	1.382	0.0076
LCD	1.722	0.0370
NORTHNESS	1.081	0.0316
TPI	1.135	0.0558

Fig. 4. Scatter plot matrix of bivariate relationships between mean air temperature and explanatory variables together with explanatory variable significance values and explanatory variable variance inflation factor values.

Joint Wald statistic $p = 0.0000^{*}$). The Jarque-Bera p value, which indicates if the model is biased, is not statistically significant ($p = 0.7494$). This means that the standardized residuals or, our under- and over-predictions of the dependent variable, are normally distributed (free from spatial autocorrelation). If underlying spatial relationships do exist, spatial autocorrelation of regression residuals would be expected in the OLS model, suggesting the misspecification of the OLS model, due to the non-stationarity of the spatial process. This was additionally confirmed with the statistically significant Global Moran's Index test (MI = 0.1013; z-score = 1.9775; $p = 0.0479$), which is a stronger indicator for spatial non-stationarity among predictors and the response variables (Table 1). The GWR calibrated F-test and the AICc values in the GWR4 software proved that there are three explanatory variables (*DIS2UA*, *LCD* and TPI) that exhibit statistically significant geographic variability (AICc > +2) even though the statistically insignificant Koenker's studentized Breusch-Pagan p-value (BP) ($p = 0.3941$), which indicated that the OLS model is designed with predictor variables that do not vary in space. However, the overall goodness-of-fit (R^2) of the OLS model was 0.73 with the adjusted R^2 value of 0.68. The adjusted R-squared is a modified version of R^2 that has been adjusted for the number of predictors in the model. The adjusted R^2 increases only if the new term improves the model more than would be expected by chance. Additionally, the OLS model performance was measured with the AICc value of −21.80. In order to improve the OLS prediction, a semiparametric GWR model, which allows for the local relationships between dependent and explanatory variables to change across the study area, were employed further on (Table 2). Three local (*DIS2UA*, *LCD* and *TPI*) and two global (*BVOL* and *NORTHNESS*) explanatory variables predicted Ljutomer's UHI intensity and morphology with a significant improvement, although the signs of the regression coeficients are the same in both the OLS and semiparametric GWR models. The adjusted R^2 is 16% better (0.84) compared to the OLS model (0.68) as well as the AICc value of the semiparametric GWR, which has decreased by 13.66 (−35.46).

The statistical comparison between the two models revealed that there is a significant improvement ($F = 4.07$; $p = 0.00013$) in UHI prediction in Ljutomer by applying the semiparametric GWR method (Table 3). The simulated residual of the GWR model (0.41) is less than that of the global mode (1.21). Generally, the spatial randomness of the residual value, as well as the magnitude of the cumulative residual, is employed as a diagnostic measure of the regression model. Accordingly, the semiparametric GWR model gives a smaller global Moran index (MI = −0.05; $p = 0.6004$) than that from the OLS model (MI = 0.10; $p = 0.0479$), suggesting more random spatial patterns in the returned residuals (Fig. 5).

The mean values of the local regression coefficients *DIS2UA* and *LCD* are negative (Table 2), implying inverse relationships between the response variable and those explanatory variables. Also *NORTHNESS*, as a global explanatory variable, has a negative relation to mean air temperature in both models. In contrast, there are positive relationships between mean air temperature and the explanatory variables *BVOL* (global) and *TPI* (local). The surface of

Table 2
The slope parameters and summary of results from the semiparametric GWR model analysis.

GWR diagnostics:

Fixed (Global) coefficients:

Variable	Estimate	Standard error	*t*(Estimate/SE)
NORTHNES	−0.048829	0.020414	−2.391963
BVOL	0.042267	0.023973	1.763114

Local coefficients:

Variable	Mean	STD	Min	Max	Lwr quartile	Median	Upr quartile
Intercept	1.6733	0.0623	1.5754	1.8445	1.6758	1.7019	1.7395
DIS2UA	−0.1842	0.0845	−0.3740	−0.0467	−0.2754	−0.1871	−0.1037
LCD	−0.0273	0.0875	−0.1583	0.1458	−0.1150	−0.0351	0.0550
TPI	0.0066	0.0680	−0.1960	0.1087	−0.0277	0.0004	0.0679

Bandwidth size:	6.9392	Classic AIC:	−55.9437
Residual sum of squares:	0.4095	AICc:	−35.4608
Effective number of parameters (mode: trace(S)):	15.8002	BIC/MDL:	−24.8608
Effective number of parameters (variance: trace(S′S)):	12.3031	CV:	0.0232
Degree of freedom z(mode: n − trace(S)):	31.1998	R squared:	0.9069
Degree of freedom (mode: n − 2trace(S)) + trace(S′S)):	27.7027	Adjusted R squared:	0.8396
ML based sigma estimate:	0.0933	Moran index (MI):	−0.0517
Unbiased sigma estimate:	0.1216	Moran index Probability (p-value):	0.6004
−2 log-likelihood:	89.5442		

Table 1
Diagnosis of the OLS analysis.

OLS regression results:

Variable	Estimate	Standard error	*t*(Est/SE)	Prob	Robust SE	Robust *t*	Robust Pr
Intercept	1.6886	0.0251	67.1462	0.0000	0.0443	41.2372	0.0000
DIS2UA	−0.1277	0.0257	−4.9651	0.0000	0.0002	−4.0788	0.0002
BVOL	0.0821	0.0293	2.8043	0.0076	0.0000	4.0736	0.0002
LCD	−0.0701	0.0325	−2.1552	0.0370	0.0780	−1.6872	0.0992
NORTHNESS	−0.0576	0.0259	−2.2257	0.0316	0.0334	−2.5974	0.0130
TPI	0.0517	0.0263	1.9681	0.0558	0.0041	2.4492	0.0187

OLS diagnostic information

Residual sum of squares:	1.2086	Joint F-Statistic Value:	21.6417
Number of parameters:	6	Joint F-Statistic Probability (p-value):	0.0000
ML based global sigma estimate:	0.1604	Wald Statistic:	105.4826
Unbiased global sigma estimate:	0.1717	Wald Statistic Probability (p-value):	0.0000
−2 log-likelihood:	−38.6728	Koenker's studentized Breusch-Pagan Statistic:	5.1819
Classic AIC:	−24.6728	Koenker (BP) Statistic Probability (p-value):	0.3941
AICc:	−21.8010	Jarque-Bera Statistic:	0.5768
BIC/MDL:	−11.7218	Jarque-Bera Probability (p-value):	0.7495
CV:	0.0359	Moran Index (MI):	0.1031
R square:	0.7252	Moran Index Probability (p-value):	0.0479
Adjusted R square:	0.6840		

Table 3
Comparison between the OLS and the semiparametric GWR models.

GWR ANOVA table:					
Source	SS	DF	MS	F	*p*-value
Global Residuals	1.209	41			
GWR Improvement	0.799	13.297	0.06		
GWR Residuals	0.409	27.703	0.015	4.0660	0.0001

local estimated coefficients and the statistically significant local t-values ($\alpha = 0.10$) are presented in Fig. 5, as well as the local R^2. Unlike the OLS model, the spatial pattern of the local goodness-of-fit measure in the GWR model shows spatial differentiation, with values from 0.68 to 0.92, characterized by higher values in city surroundings and lower values in the city center, reflecting that the GWR model has good ability to characterize spatial non-stationarity (Fig. 5). The *DIS2UA* local estimate has a negative influence on mean air temperature in the eastern part of the city and a slightly higher, but still negative, influence in the southern and eastern part, whereas it is not significant in the city center or in the northern, mainly industrial part of Ljutomer. In the southern and northern part of Ljutomer, the *LCD* estimated coefficient is in significant negative relation, and contrastingly, in the eastern rural surrounding of the city, in a slightly positive relation. *LCD* is an insignificant influence on the mean air temperature in most of the city built-up area. *TPI* has a significant positive influence on the response variable mainly in the southern part on the southern slopes of nearby Kamenščak hill. The statistically significant negative influence is detected only in the lowest part of the city, between the Ščavnica river and its regulation channel (Fig. 5).

However, the over- and under-predictions of the semiparametric GWR model are normally distributed; there is no spatial autocorrelation in the standardized residuals (Moran's Index *p*-value = 0.6004). Their spatial distribution is presented in Fig. 5. Some minor under-predictions occured in the non-urban areas between the Ščavnica river and its regulation channel and also on the northern slopes of Kamenščak hill. Over-predictions are associated with the higher elevation directly on the southern slopes of Kamenščak hill, and some also appear in the rural area in an eastern

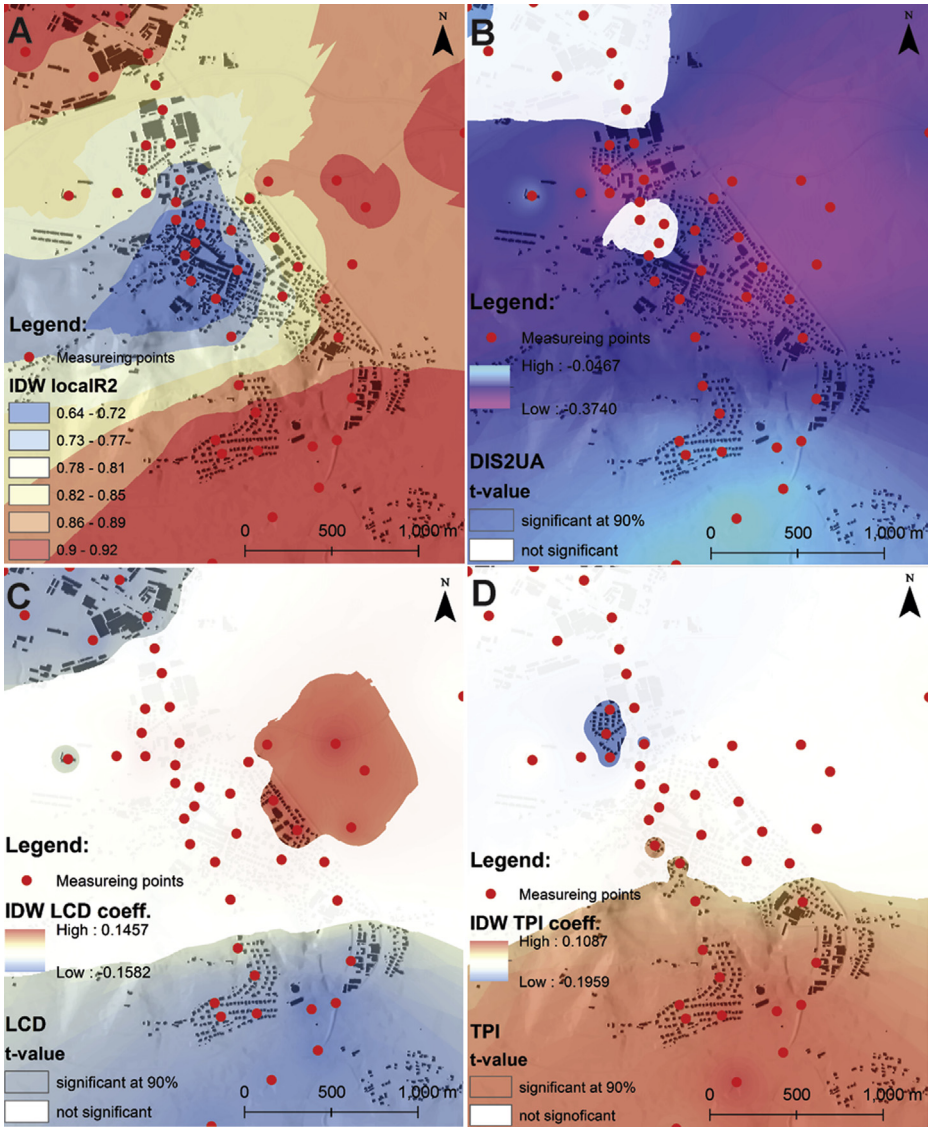

Fig. 5. Local R^2 values for local explanatory variables (*DIS2UA, LCD AND TPI*) (A) with local regression coefficients and corresponding statistically significant local t-values ($\alpha = 0.10$) (B, C and D).

direction from the railway. Differences in observed and predicted air temperature are shown in red (Fig. 6). It should be pointed out that the greatest difference has a scale of only 0.2 °C. For 40% of the points, the semiparametric GWR model predicts the exact mean air temperature, for 89% of the points cumulatively, with an maximum error of 0.1 °C and only in 11%, with an error of 0.2 °C.

The comparison between predicted and observed mean air temperature in the city, estimated using semiparametric GWR with an adaptive kernel type and Akaike's Information Criterion for the bandwidth method, showed an overall fitting performance of 91% (Fig. 7). In this regard, we were able to model the UHI phenomenon of a small city with five response variables (three local and two global) with quite remarkable agreement.

Discussion

Most recent studies of the UHI phenomenon were done in large metropolitan areas or major cities across the globe, mainly based on remotely sensed satellite imagery, producing land surface temperature (LST) as the main variable indicating its intensity and morphology (Buyantuyev and Wu 2010; Choi et al., 2012; Li et al., 2009; Li et al., 2010; Rinner & Hussain, 2011; Rogan et al., 2013; Stewart et al., 2011; Zakšek & Oštir, 2012; Zhang et al., 2013). In smaller urban areas, mobile (in-situ) measurements of climate parameters, which enable reliable modeling, are still widespread (e.g., Balazs et al., 2009; Moreno-Garcia, 1994; Oke & Fuggle, 1972). Arnfield (2003) pointed out that UHI or the urban heat island archipelago (Klysik & Fortuniak, 1999; Park, 1986) is a general characteristic of medium and large urban areas.

However, this study proves that even small cities can develop specific microclimatic conditions which are caused by the same

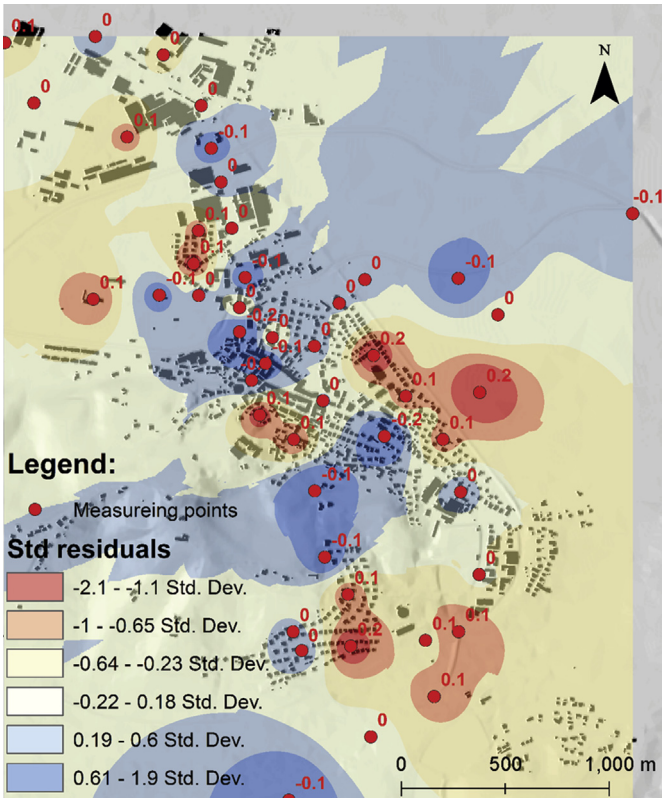

Fig. 6. Standardized residuals of the semiparametric GWR model, showing under (blue color) and over (red color) predictions. The red numbers represent differences between observed and predicted mean air temperatures at each measuring point.

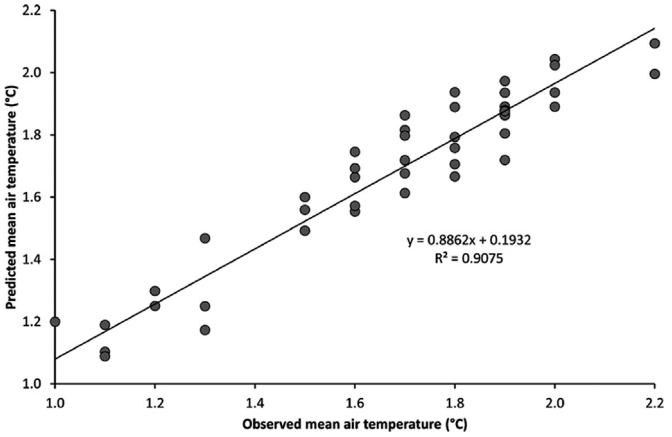

Fig. 7. Scatter diagram of observed and GWR-computed mean air temperatures at measuring points.

natural conditions. As early as 1973, Oke had pointed out that UHI magnitude is related to city size, especially under cloudless sky conditions, on a regional basis, although individual cities may be impacted by such local factors as proximity to large water bodies or prevailing winds (Oke, 1995; Figuerola & Mazzeo, 1998). Significant differences in mean air temperature, in winter between urban (3.1 ± 5.1 °C) and suburban areas (2.4 ± 5.1 °C) of Ljutomer, compared to the rural surroundings (2.3 ± 5.1 °C), were recognized. The main reason for the similarities in mean air temperature between rural and suburban areas lies in the placement (microlocation) of the measuring station located in the city surroundings, which was installed at a slightly higher elevation (214 m a.s.l.), compared to the city (172 m a.s.l.), probably extending into a thermal belt. The densely built-up areas of Ljutomer are on average 1 °C warmer than the rural surroundings. The intensity of the UHI event in small cities is, of course, measured on a smaller scale but can nevertheless affect human wellbeing and comfort throughout the year (i.e., in our case the maximum measured difference in air temperature, under cloudless sky conditions, between rural and urban areas was 6 °C). In this regard, higher winter air temperatures in cities should be considered as beneficial for human wellbeing, presenting the UHI phenomenon in this case from a positive angle. The most intensive warming in Ljutomer occurs mostly in the old medieval center stretching to the northern industrial part of the city and is strongly positively related to the *BVOL* variable. However, *DIS2UA*, *BVOL*, *LCD*, *NORTHNESS* and *TPI* could explain most of the UHI intensity and morphology in this small city example. Mean air temperature in Ljutomer decreases with the increment of *DIS2UA* and *LCD*, as expected. Higher Shannon's index values, indicating higher *LCD*, are associated with lower air temperatures, owing to different physical properties of the surrounding surfaces (albedo, heat capacity, evapotranspiration, soil water content etc.). Topographic variability can interfere with the regular UHI pattern. Consequently, many statistical models of UHIs are developed in cities which are situated on a flat plain (i.e. Balazs et al., 2009; Li et al., 2009; Stewart et al., 2011; Szymanowski & Kryza, 2012; Unger et al., 2011 ecc.). Because Lutomer is developed around and partway on Kamenščak hill, *NORTHNESS* and *TPI* were included in the semiparametric GWR model in order to explain the mean air temperature at the elevated measuring points. It should be pointed out that aspect does not directly affect temperatures if measurements are taken before sunrise. However, the main reason for choosing the variable *NORTHNESS* in our case is the fact that the mobile measurements were carried out at 7:00 am, even in mid-February and in March 2009, where the sun was high

enough to influence some results, in particular those on the exposed slopes of Kamenščak hill. Both β coefficients (negative *NORTHNESS* and positive *TPI*) proved that on the southern slopes of Kamenšak hill a temperature inversion belt develops as a consequence of a cold air drainage flow into the valley of the Kostanjevica watercourse (in the S direction) and intensive warming of the southern exposed area in forenoon hours. The statistically significant variations of local explanatory variable estimates excuses the usage of the GWR method. The latter has become a useful approach for exploring the spatial non-stationary and scale-dependent phenomena that occur within the processes and patterns of ecology and geography (Li et al., 2010; Zhang, Gove, & Heath, 2005).

In recent years, there has been increasing research interest in the effects of the UHI and in related influence factors, and many regression relationships have been developed (Li et al., 2010). The GWR model not only has a better fit performance than the global OLS model, but also provides local detailed information about how the spatial variation of mean air temperature is affected by geographical and ecological factors. Holt and Lo (2008) concluded that some limitations for the GWR model still exist; it assumes spatial non-stationarity for all variables, while in reality some natural processes may exhibit spatial stationarity, especially in homogenous regions. Mei, Wang, and Zhang (2006) presented an alternative approach by extending GWR to a mixed, geographically weighted regression (MGWR), which is now integrated in the form of a semiparametric GWR in the GWR4 software, developed by Nakaya et al. (2014) and combines globally fixed terms and locally varying terms of explanatory variables simultaneously. In general, the statistical GWR model obtained from measurements cannot easily be transferred elsewhere where there are only few or no measurements. On the other hand, the OLS model may be inferior regarding distinct locations, owing to instationarities of transfer functions in space. However, OLS can much more easily be transferred to other places, since it exploits statistical relations over all the data in the region of interest, and can therefore be applied even beyond the geographical limits of the measurements in cases where the physical settings remain similar, which is a big advantage over the GWR method, which does not allow such global usage.

Our findings about the homogenous UHI phenomenon in Ljutomer raise the question of whether the arrangement between urban and non-urban areas is really appropriate. Urban green space, such as forests or parks, can eases UHI effects through increased latent heat exchange (evapotranspiration), shading (preventing incoming solar radiation from heating the surrounding buildings and surfaces) and wind speed reduction (Akbari, Pomerantz, & Taha, 2001; Buyantuyev & Wu, 2010; ; Jonsson, 2004; Spronken-Smith & Oke, 1998). Choi et al. (2012) reported that the ratio of urban heat area to urban cooling area increases with distance from a green space boundary and pointed out that urban green space plays an important role in mitigating urban heating, especially in central areas. Rogan et al. (2013) measured a 0.7 °C increase in LST after removing 10% of the tree canopy, whereas a 10% increase in sub-canopy impervious surface area exposed by tree loss caused a 1.66 °C increase in LST. However, because the maximum cooling distance of urban green space is rather small (Feyisa et al., 2014), it is therefore even more important in small cities where dispersed green areas could neutralize elevated air temperatures caused by the UHI effect. In the case of Ljutomer, the mitigating climate effect of the green area is insignificant, because of its small size, limited to just two small city parks and the sport-recreation area across the Ščavnica river. The relationship between land use, the UHI effect, and regional climate change requires that the underlying mechanisms, patterns, and processes of land conversion, as well as the response of urban climate should be addressed through official decision-making processes (Zhang et al., 2013).

Conclusion

It is not just in big cities or agglomerations that the so called urban climate is evident, but even in small towns. Impervious urban cover experiences higher temperatures compared to non-impervious cover, as a result of the changed energy and water balance caused by human alterations and activities in cities. An UHI does develop over Ljutomer, with a significant hot spot in the city center, partly extending to the industrial area in the north. Its intensity and morphology are mainly explained with explanatory variables like distance to urban area, building volume per area, land-cover diversity, northness and topographic position index. The significant geographic variability of the explanatory variables distance to urban area, land-cover diversity, topographic position index and local stationarity of variables building volume per are and northness, excuses the usage of local mixed regression models like the semiparametric GWR. Although the signs of the regression coefficients are the same in both the OLS and the semiparametric GWR models, the explanatory power of the latter is stronger, and is characterized by higher adjusted R^2 values (an increase of 16%), reduction of AICc (a 13.66 decrease), lower Moran index value (0.15 decrease) and smaller residual values. However, as a disadvantage to the global OLS model, local regression models are still case specific and cannot easily be transferred elsewhere in the geographical space. In this research the semiparametric GWR method was tested on the smallest scale so far published and even then produced very good results.

The homogeneity of the UHI phenomenon is the result of the concentrated city structure and the arrangement between urban and non-urban areas. Topographic effects alter UHI intensity and morphology in Ljutomer in particular on the southern slopes of hill Kamenščak where temperature inversion is frequently present in winter time. In general, our findings support urban planning and management strategies to mitigate the negative effects or to take benefit from positive effects of built-up area heating in both large and small cities across the globe, following the principles of long-term, sustainable development.

References

Akbari, H., Pomerantz, M., & Taha, H. (2001). Cool surfaces and shade trees to reduce energy use and improve air quality in urban areas. *Solar Energy, 70*(3), 295–310.

Alcoforado, M. J., & Andrade, H. (2006). Nocturnal urban heat island in Lisbon (Portugal): main features and modelling attempts. *Theoretical and Applied Climatology, 84*, 151–159.

Arnfield, A. J. (2003). Two decades of urban climate research: a review of turbulence, exchanges of energy and water, and the urban heat island. *International Journal of Climatology, 23*, 1–26.

ARSO. (2006). *Podnebne razmere v Slovenji (obdobje 1971-2000)* [*Climate conditions in Slovenia from 1971 to 2000*]. Available at http://www.arso.gov.si/vreme/podnebje/podnebne_razmere_Slo71_00.pdf Accessed on 12.03.14.

Balazs, B., Unger, J., Gal, T., Sümeghy, Z., Geiger, J., & Szegedi, S. (2009). Simulation of the mean urban heat island using 2D surface parameters: empirical modelling, verificaton and extension. *Meteorological Applications, 16*, 275–287.

Belec, B. (1995). Ljutomer. In M. Orožen Adamič, D. Perko, & D. Kladnik (Eds.), *Krajevni leksikon Slovenije, (Lexicon of Slovenian settlements)*. Ljubljana: DZS.

Bottyan, Z., Kircsi, A., Szegedi, S., & Unger, J. (2005). The relationship between built-up areas and the spatial development of the mean maximum urban heat island in Debrecen, Hungary. *International Journal of Climatology, 25*(3), 405–418.

Bottyán, Z., & Unger, J. (2003). A multiple linear statistical model for estimating mean maximum urban heat island. *Theoretical and Applied Climatology, 75*, 233–243.

Brunsdon, C., Fotheringham, A. S., & Charlton, M. E. (1996). Geographically weighted regression: a method for exploring spatial nonstationarity. *Geographical Analysis, 28*, 281–298.

Brundson, C., Fotheringham, S. A., & Charlto, M. (1999). Some notes on parametric significance tests for geographically weighted regression. *Journal of Regional Science, 39*, 497–524.

Buechley, R. W., Truppi, L. E., & Van Brugg, J. (1972). Heat island = death island? *Environmental Research, 5*(1), 85–92.

Buyantuyev, A., & Wu, J. (2010). Urban heat islands and landscape heterogeneity: linking spatiotemporal variations in surface temperatures to land-cover and socioeconomic patterns. *Landscape Ecology, 25*, 17–33.

Čadež, M. (1949). O tipovima vremena, (About weather types). *Hidrometeorološki glasnik, 2*, 88–95.

Choi, H. A., Lee, W. K., & Byun, W. H. (2012). Determining the effect of green spaces on urban heat distribution using satellite imagery. *Asian Journal of Atmospheric Environment, 6-2*, 127–135.

Duckworth, F. S., & Sandberg, J. S. (1954). The effect of cities upon horizontal and vertical temperature gradients. *Bulletin of the American Meteorological Society, 3*, 198–207.

Dutilleul, P., & Legendre, P. (1993). Spatial heterogeneity against heteroscedasticity: an ecological paradigm versus a statistical concept. *OIKOS, 66*, 152–171.

ESRI. (2010). *ArcGIS Desktop: Release 9.3*. Environmental Systems Research Institute, Redlands.

Farber, S., & Paez, A. (2007). A systematic investigation of cross-validation in GWR model estimation: empirical analysis and Monte Carlo simulations. *Journal of Geographical Systems, 9*, 371–396.

Feyisa, G. L., Dons, K., & Meilby, H. (2014). Efficiency of parks in mitigating urban heat island effect: an example from Addis Ababa. *Landscape and Urban Planning, 123*, 87–95.

Fezer, F. (1994). *Das Klima der Städte* [*City Climate*]. Gotha: Justus Perthes Verlag.

Figuerola, P., & Mazzeo, N. (1998). Urban-rural temperature differences in Buenos Aires. *International Journal of Climatology, 18*, 1709–1723.

Foody, G. M. (2003). Geographical weighting as a further refinement to regression modelling: an example focused on the NDVI-rainfall relationship. *Remote Sensing of Environment, 88*, 283–293.

Foody, G. M. (2004). Spatial nonstationary and scale-dependency in the relationship between species richness and environmental determinants for the sub-Saharan endemic avifauna. *Global Ecology and Biogeography, 13*, 315–320.

Foody, G. M. (2005). Clarifications on local and global data analysis. *Global Ecology and Biogeography, 14*, 99–100.

Fotheringham, A. S., Brunsdon, C., & Charlton, M. (2002). *Geographically weighted regression: The analysis of spatially varying relationships*. Chichester: Wiley.

Gallo, K. P., Owen, T. W., Easterling, D. R., & Jamason, P. F. (1999). Temperature trends of the U.S. Historical Climatology Network based on satellite-designated land use/land cover. *Journal of Climate, 12*(5), 1344. http://dx.doi.org/10.1175/1520-0442(1999)012<2.0.CO;2.

Gartland, L. (2008). *Heat island: Understanding and mitigating heat in urban areas*. London/Sterling, VA: Earthscan.

Grigillo, D., Kosmatin Fras, M., & Petrovič, D. (2011). Automatic extraction and building change detection from digital surface model and multispectral orthophoto. *Geodetski vestnik, 55*(1), 28–45.

Grimm, N. B., Faeth, S. H., Golubiewski, N. E., Redman, C. L., Wu, J., Bai, X., et al. (2008). Global change and the ecology of cities. *Science, 319*, 756–760.

GURS. (2007). *Katastrski načrt občine Ljutomer* [*Vectorized land register of the municipality of Ljutomer*]. Geodetska Uprava Republike Slovenije (The surveying and mapping authority of the Republic of Slovenia, Ministry of Infrastructure and Spatial Planning), Ljubljana.

GURS. (2010). *Digitalni model višin 5×5 m* [*Digital elevation model 5×5 m*]. Geodetska Uprava Republike Slovenije (The surveying and mapping authority of the Republic of Slovenia, Ministry of Infrastructure and Spatial Planning), Ljubljana.

GURS. (2014). *Kataster stavb (The national register of buildings)*. Geodetska Uprava Republike Slovenije (The surveying and mapping authority of the Republic of Slovenia, Ministry of Infrastructure and Spatial Planning), Ljubljana.

Hinkel, K. M., Nelson, F. E., Klene, A. E., & Bell, J. H. (2003). The urban heat island in winter at Barrow, Alaska. *International Journal of Climatology, 23*, 1889–1905.

Holt, J. B., & Lo, C. P. (2008). The geography of mortality in the Atlanta metropolitan area. *Computers, Environment and Urban System, 32*, 149–164.

Howard, L. (1820). *Climate of London deduced from meteorological observations* (Vols. 1–3). London: Harvey and Darton.

Jenness, J., Brost, B., & Beier, P. (2013). *Land facet corridor designer*. Available from http://www.jennessent.com/downloads/Land_Facet_Tools_A4.pdf Accessed on 12.02.14.

Jonsson, P. (2004). Vegetation as an urban climate control in the subtropical city of Gaborone, Botswana. *International Journal of Climatology, 24*, 1307–1322.

Johnson, D. P., & Wilson, J. S. (2013). The socio-spatial dynamic of extreme urban heat events: the case of heat-related deaths in Philadelphia. *Applied Geography, 29*, 419–434.

Klysik, K., & Fortuniak, K. (1999). Temporal and spatial characteristics of the urban heat island of Lodz, Poland. *Atmospheric Environment, 33*, 3885–3895.

Kottek, M., Grieser, J., Beck, C., Rudolf, B., & Rubel, F. (2006). World map of the Köppen-Geiger climate classification updated. *Meteorologische Zeitschrift, 15*(3), 259–263.

Landsberg, H. E. (1981). *General climatology – World survey of climatology* (Vol. 3). Amsterdam-Oxford-New York: Elsevier Scientific Publishing Company.

Li, J. J., Wang, X. R., Wang, X. J., Ma, W. C., & Zhang, H. (2009). Remote sensing evaluation of urban heat island and its spatial pattern of the Shanghai metropolitan area, China. *Ecological Complexity, 6*, 413–420.

Li, S., Zhao, Z., Miaomaio, X., & Wang, Y. (2010). Investigating spatial non-stationary and scale-dependent relationships between urban surface temperature and environmental factors using geographically weighted regression. *Environmental Modelling & Software, 25*, 1789–1800.

Lillesand, T. M., & Kiefer, R. W. (1987). *Remote sensing and image interpretation*. New York: John Wiley and Sons.

Maselli, F. (2002). Improved estimation of environmental parameters through locally calibrated multivariate regression analysis. *Photogrammetric Engineering & Remote Sensing, 68*(11), 1163–1171.

Mei, C. L., Wang, N., & Zhang, W. X. (2006). Testing the importance of the explanatory variables in a mixed geographocally weighted regression model. *Environment and Planning A, 38*, 587–598.

Moreno-Garcia, M. C. (1994). Intensity and form of the urban heat island in Barcelona. *International Journal of Climatology, 14*(6), 705–710.

Nakaya, T., Charlton, M., Fotheringham, S., & Brundson, C. (2014). *GWR4 version 4.0.80. Application for geographically weighted regression modelling*. National Centre for Geocomputation, National University of Ireland MAynooth nad Department of Geography, Ritsumeikan University, Japan.

Ogrin, D. (2009). Spreminjanje podnebja v Prekmurju po 2. svetovni vojni [The change in climate in Prekmurje after the 2nd World war]. In T. Kikec (Ed.), *Pomurje: trajnostni regionalni razvoj ob reki Muri : zbornik povzetkov* (p. 46). Ljubljana: Zveza geografov Slovenije; Murska Sobota: Društvo geografov Pomurja.

Oke, T. R. (1973). City size and the urban heat island. *Atmospheric Environment, 7*(8), 769–779.

Oke, T. R. (1981). Canyon geometry and the nocturnal urban heat island: comparison of scale model and field observations. *Journal of Climatology, 1*(3), 237–254.

Oke, T. R. (1982). The energetic basis of the urban heat island. *Quarterly Journal of the Royal Meteorological Society, 108*, 1–24.

Oke, T. R. (1987). *Boundary layer climates* (2nd ed.). London, UK: Routledge.

Oke, T. R. (2004). *Initial guidance to obtain representative meteorological observation sites,WMO/TD 1250*.

Oke, T. R., & Fuggle, R. F. (1972). Comparison of urban/rural counter and net radiation at night. *Boundary-Layer Meteorology, 2*(3), 290–308.

Oke, T. R. (1995). The heat iskand of the urban boundary layer: characteristics, causes and effects. In J. E. Cermark, et al. (Eds.), *Wind climate in cities* (pp. 81–107). Dordrecht: Kluwer Academic Publisher.

Oke, T. R., Spronken-Smith, R. A., Jauregiu, E., & Grimmond, C. S. B. (1999). The energy balance of central Mexico City during the dry season. *Atmospheric Environment, 33*, 3919–3930.

Park, H. S. (1986). Features of the heat island in Seoul and its surrounding cities. *Atmospheric Environment, 20*, 1859–1866.

Propastin, P., Kappas, M., & Erasmi, S. (2008). Application of geographically weighted regression to investigate the impact of scale on prediction uncertainty by modelling relationship between vegetation and climate. *International Journal of Spatial Data Infrastructures Research, 3*, 73–94.

R Development Core Team. (2008). *R: A language and environment for statistical computing*. Vienna, Austria: R Foundation for Statistical Computing, ISBN 3-900051-07-0. http://www.Rproject.org.

Rinner, C., & Hussain, M. (2011). Toronto's urban heat island - exploring the relationship between land use and surface temperature. *Remote Sensing, 3*, 1251–1265.

Roberts, D. W. (1986). Ordination on the basis of fuzzy set theory. *Vegetatio, 66*, 123–131.

Rogan, J., Ziemer, M., Martin, D., Ratick, S., Cuba, N., & DeLauer, V. (2013). The impact of tree cover loss on land surface temperature: a case study of central Massachusetts using Landsat Thematic Mapper thermal data. *Applied Geography, 45*, 49–57.

Rosenfeld, A. H., Akbari, H., Romm, J. J., & Pomerantz, M. (1998). Cool communities: strategies for heat island mitigation and smog reduction. *Energy and Buildings, 28*, 51–62.

Roth, M. (2002). Effects of cities on local climates. In *Proceedings of Workshop of Institute for Global Environment Studies/Asia-Pacific Network (IGES/APN) Mega-city Project. Kitakyushu, Japan*.

Shannon, C. E., & Weaver, W. (1963). *The mathematical theory of communication*. Urbana: University of Illinois Press.

Sheng, J., Wilson, J. P., & Lee, S. (2009). Comparison of land surface temperature (LST) modeled with a spatially distributed solar radiation model (SRAD) and remote sensing data. *Environmental Modelling & Software, 24*, 436–443.

Souch, C., & Grimmond, C. S. B. (2006). Applied climatology: urban climate. *Progress in Physical Geography, 30*, 270–279.

Spronken-Smith, R. A., & Oke, T. R. (1998). The thermal regime of urban parks in two cities with different summer climates. *International Journal of Remote Sensing, 19*, 2085–2104.

Stewart, N., Stenz, T., & Gottinger, P. (2011). *Modeling the land surface temperature of the Kansas city metro area*. Geo 578 GIS Applications. Available at http://minds.wisconsin.edu/handle/1793/55292?show=full Accessed 12.03.14.

Stull, R. B. (1988). *An introduction to boundary layer meterology*. Dordrecht: Kluwer Academic.

Su, Y.-F., Foody, G. M., & Cheng, K.-S. (2012). Spatial non-stationarity in the relationships between land cover and surface temperature in an urban heat island and its impact on thermally sensitive populations. *Landscape and Urban Planning, 107*, 172–180.

Svensson, M. K., Eliasson, I., & Holmer, B. (2002). A GIS based empirical model to simulate air temperature variations in the Göteborg urban area during the night. *Climate Research, 22*, 215–226.

Szymanowski, M., & Kryza, M. (2012). Local regression models for spatial interpolation of urban heat island-an example from Wroclaw, SW Poland. *Theoretical and Applied Climatology, 108*, 53–71.

Tucker, C. J. (1979). Red and photographic infrared linear combinations for monitoring vegetation. *Remote Sensing of Environment, 8*, 127–150.
Unger, J. (2004). Intra-urban relationship between surface geometry and urban heat island: review and new approach. *Climate Research, 27*(3), 253–264.
Unger, J., Savić, S., & Gal, T. (2011). Modelling of the annual mean urban heat island pattern for planning of representative urban climate station network. *Advances in Meteorology, 11*, 1–9.
Upmanis, H., Eliasson, I., & Lindqvist, S. (1998). The influence of green areas on nocturnal temperatures in a high latitude city (Göteborg, Sweden). *International Journal of Climatology, 18*, 681–700.
Vicente-Serrano, S. M., Cuadrat-Prats, J. M., & Saz-Sánchez, M. A. (2005). Spatial patterns of the urban heat island in Zaragoza (Spain). *Climate Research, 30*, 61–69.
Voogt, J. A., & Oke, T. R. (2003). Thermal remote sensing of urban areas. *Remote Sensing of Environments, 86*, 370–384.
Wu, J. (2008). Making the case for landscape ecology: an effective approach to urban sustainability. *Landscape Journal, 27*, 41–50.
Zakšek, K., & Oštir, K. (2012). Downscaling land surface temperature for urban heat island diurnal cycle analyses. *Remote Sensing of Environment, 117*, 114–124.
Zhang, L., Gove, J. H., & Heath, L. S. (2005). Spatial residual analysis of fix modeling techniques. *Ecological Modelling, 186*, 154–177.
Zhang, H., Qi, Z. F., Ye, X. Y., Cai, Y. B., Ma, W. C., & Chen, M. N. (2013). Analysis of land use/land cover change, population shift, and their effects on spatiotemporal patterns of urban heat islands in metropolitan Shanghai, China. *Applied Geography, 44*, 121–133.
Zhou, X., & Wang, Y.-W. (2001). Dynamics of land surface temperature in response to land-use/cover change. *Geographical Research, 49*, 23–36.
Žiberna, I. (2006). Trendi temperatur zraka v Mariboru kot posledica razvoja mestnega toplotnega otoka [Air temperature trends in Maribor as a consequence of the development of the urban heat islands]. *Revija za geografijo, 1–1*, 81–98.